

# Tracking Sports Players with Context-Conditioned Motion Models

Jingchen Liu<sup>1</sup>

Peter Carr<sup>2</sup>

Robert T. Collins<sup>1</sup>

Yanxi Liu<sup>1</sup>

<sup>1</sup>The Pennsylvania State University

<sup>2</sup>Disney Research Pittsburgh

{jingchen, collins, yanxi}@cse.psu.edu

peter.carr@disneyresearch.com

## Abstract

We employ hierarchical data association to track players in team sports. Player movements are often complex and highly correlated with both nearby and distant players. A single model would require many degrees of freedom to represent the full motion diversity and could be difficult to use in practice. Instead, we introduce a set of Game Context Features extracted from noisy detections to describe the current state of the match, such as how the players are spatially distributed. Our assumption is that players react to the current situation in only a finite number of ways. As a result, we are able to select an appropriate simplified affinity model for each player and time instant using a random decision forest based on current track and game context features. Our context-conditioned motion models implicitly incorporate complex inter-object correlations while remaining tractable. We demonstrate significant performance improvements over existing multi-target tracking algorithms on basketball and field hockey sequences several minutes in duration and containing 10 and 20 players respectively.

## 1. Introduction

Multi-target tracking has been a difficult problem of broad interest for years in computer vision. Surveillance is perhaps the most common scenario for multi-target tracking, but team sports is another popular domain that has a wide range of applications in strategy analysis, automated broadcasting, and content-based retrieval. Recent work in pedestrian tracking has demonstrated promising results by formulating multi-target tracking in terms of data association [1, 4, 7, 18, 23, 25, 27, 29]: a set of potential target locations are estimated in each frame using an object detector, and target trajectories are inferred by linking similar detections (or tracklets) across frames. However, if complex inter-tracklet affinity models are used, the association problem quickly becomes NP-hard.

Tracking players in team sports has three significant differences compared to pedestrians in surveillance. (1) the appearance features of detections are less discriminative

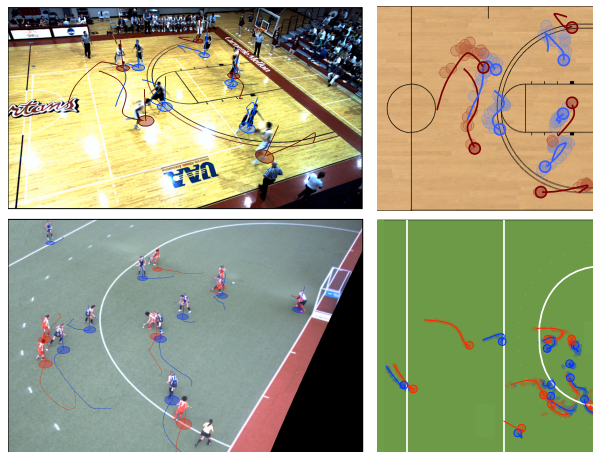


Figure 1. Motion Models. A player’s future motion is contingent on the current game situation. The global distribution of players often indicates which team is attacking, and local distributions denote when opposing players are closely following each other. We use contextual information such as this to create a more accurate motion affinity model for tracking players. The overhead views of basketball and field hockey show the input detections and corresponding ground truth annotations. Player trajectories are strongly correlated with both nearby and distant players.

because players on the same team will be visually similar. The distinguishing characteristics between teammates are primarily position and velocity; (2) pedestrians tend to move along straight lines at constant speed, whereas sports players move in more erratic fashions; (3) although pedestrians deviate to avoid colliding with each other, the motions between pedestrians are rarely correlated in complex ways (some scenarios, like sidewalks, may contain a finite number of common global motions). The movements of sports players, on the other hand, are strongly correlated both locally and globally. For example, opposing players may exhibit strong local correlations when ‘marking’ each other (such as one-on-one defensive assignments). Similarly, players who are far away from each other move in globally correlated ways because they are reacting to the same ball.

Simple, independent motion models have been popular for pedestrian tracking because they limit the complexity of

the underlying inference problem [7]. However, the models may not always characterize the motion affinity between a pair of tracklets accurately. Brendel *et al.* [4] modeled inter-target correlations between pedestrians using *context* which consisted of additional terms in the data association affinity measure based on the spatiotemporal properties of tracklet pairs. Following this convention, we will describe correlations between player movements in terms of *game context*. Much like the differences between the individual target motions in surveillance and team sports, game context is more complex and dynamic compared to context in surveillance. For example, teams will frequently gain and lose possession of the ball, and the motions of all players will change drastically at each turnover.

Because a player’s movement is influenced by multiple factors, the traditional multi-target tracking formulation using a set of independent autoregressive motion models is a poor representation of how sports players move. However, motion affinity models conditioned on multiple targets (and that do not decompose into a product of pairwise terms) make the data association problem NP-hard [7]. In this work, we show how data association is an effective solution for sports player tracking by devising an accurate model of player movements that remains tractable by conditioning on features describing the current state of the game, such as which team has possession of the ball. One of our key contributions is a new set of broad *game context features* (GCF) for team sports and their estimation from noisy player detections. As a result, we can better assess the affinity between trajectory segments by implicitly modeling complex interactions through a random decision forest based on track and game context features. We demonstrate the ability to track 20 players in over 30 minutes of international field hockey matches, and 10 players in 5 minutes of college basketball.

## 2. Related Work

Recent success in pedestrian tracking has posed multi-target tracking as data association: long object trajectories are found by linking together a series of detections or short tracklets. The problem of associating tracklets across time has been investigated using a variety of methods, such as the Hungarian algorithm [9, 19], linear programming [10], cost-flow networks [27], maximum weight independent sets [4], continuous-discrete optimization [3] and higher-order motion models [7]. Data association is often formulated as a linear assignment problem where the cost of linking one tracklet to another is some function of extracted features (typically motion and appearance). More recent work (discussed shortly) considers more complex association costs.

Crowds are an extreme case of pedestrian tracking where it is often not possible to see each individual in their entirety. Because of congestion, pedestrian motions are often quite similar, and crowd tracking algorithms typically estimate a

finite set of global motions. Often, the affinity for linking two tracklets together depends on how well the hypothesized motion agrees with one of the global motions. [1, 29] solve tracking in crowded structured scenes with floor fields estimation and Motion Structure Tracker, respectively. [21] uses a Correlated Topic Model for crowded, unstructured scenes.

Team sports is another relevant domain for multi-target tracking [22], with algorithms based on particle filters being extremely popular [5, 8, 13, 15, 16, 24]. However, results are quite often demonstrated only on short sequences (typically less than two minutes). Alternatively, Nillius *et al.* [17] generated a Bayes network of splitting and merging tracklets for a long ten minute soccer sequence, and found the most probable assignment of player identities using max-margin message passing.

In both pedestrian and player tracking, object motions are often assumed to be independent and modeled as zero displacement (for erratic motion) and/or constant velocity (for smooth motion governed by inertia). In reality, the locations and motions of players are strongly correlated. Pair-wise repulsive forces have been used in multi-target tracking to enforce separability between objects [2–4, 11, 26]. Recently, multi-object motion models have been used in pedestrian tracking to anticipate how people will change their trajectories to avoid collisions [18], or for estimating whether a pair of trajectories have correlated motions [4]. In team sports, Kim *et al.* [12] estimated motion fields using the velocities of tracklets to anticipate how the play would evolve, but did not use the motion fields to track players over long sequences. Zhang *et al.* [28] augmented the standard independent autoregressive motion model with a database of *a priori* trajectories manually annotated from other games.

## 3. Hierarchical MAP Association Tracking

Objects are tracked via data association by first extracting a set of detections  $\mathcal{O}$  where each detection  $\mathcal{O}_i = [\mathbf{x}_i, t_i, \mathbf{a}_i]$  consists of position, time stamp and appearance information respectively. The goal is to find the most probable set  $\mathcal{T} = \{\mathcal{T}_1, \mathcal{T}_2, \dots, \mathcal{T}_N\}$  of object trajectories where each trajectory is a temporal sequence of detections  $\mathcal{T}_n = \{\mathcal{O}_a, \mathcal{O}_b, \dots\}$

$$\mathcal{T}^* = \arg \max_{\mathcal{T}} P(\mathcal{O}|\mathcal{T})P(\mathcal{T}). \quad (1)$$

The likelihood  $P(\mathcal{O}|\mathcal{T})$  indicates how well a set of trajectories  $\mathcal{T}$  matches the observations, and the prior  $P(\mathcal{T})$  describes, in the case of sports tracking, how realistic the set of estimated player trajectories  $\mathcal{T}$  is. In multi-target tracking, the prior is often simplified to consider each trajectory

in isolation and with Markov independence

$$P(\mathcal{T}) \sim \prod_n P(\mathcal{T}_n) \quad (2)$$

$$= \prod_n \prod_t P(\mathcal{T}_n^t | \mathcal{T}_n^{t-1}), \quad (3)$$

where  $\mathcal{T}_n^t$  indicates the trajectory of the  $n$ th player at time interval  $t$ .

In team sports, the prior is a highly complex function and is not well approximated by a series of independent trajectory assessments. We maintain the formulation of conditional independence between trajectories, but condition each individual trajectory prior on a set of game context features  $\theta$  which describe the current state of the match

$$P(\mathcal{T}) \stackrel{\text{def}}{=} \prod_{n,t} P(\mathcal{T}_n^{t-1} \rightarrow \mathcal{T}_n^t | \theta). \quad (4)$$

Conditioning the individual motion models on game context implicitly encodes higher-order inter-trajectory relationships and long-term intra-trajectory information without sacrificing tractability.

### 3.1. Hierarchical Association

Because the solution space of data association grows exponentially with the number of frames, we adopt hierarchical association to handle sequences that are several minutes long (see Fig. 2).

**Low-Level Trajectories** A set  $\Upsilon$  of low-level tracklets is extracted from the detections by fitting constant velocity models to clusters of detections in 0.5s long temporal windows using RANSAC. Each  $\Upsilon_i$  represents an estimate of an object's instantaneous position and velocity (see Fig. 3).

**Mid-Level Trajectories** Similar to [9], the Hungarian algorithm is used to combine subsequent low-level trajectories into a set  $\Gamma$  of mid-level trajectories up to 60s in duration. The method automatically determines the appropriate number of mid-level trajectories, but is tuned to prefer shorter, more reliable trajectories. Generally, mid-level trajectories terminate when abrupt motions occur or when a player is not detected for more than two seconds.

**High-Level Trajectories** MAP association is equivalent to minimum cost flow in a cost flow network [27] where a vertex  $i$  is defined for each mid-level trajectory  $\Gamma_i$  and edge weights reflect the likelihood and prior in (4). Unlike the Hungarian algorithm, it is possible to constrain solutions to have exactly  $N$  trajectories by pushing  $N$  units of flow between special source  $s$  and sink  $t$  vertices (see Fig. 4). The complete trajectory  $\mathcal{T}_n$  of each player corresponds to

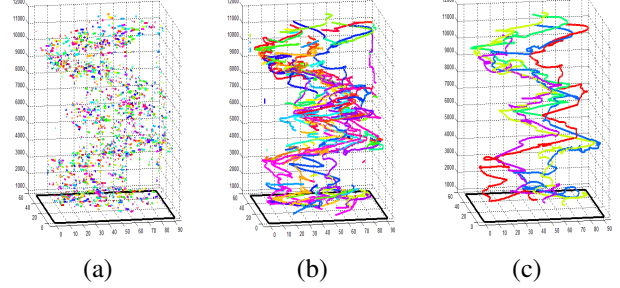


Figure 2. Hierarchical Association. (a) low-level tracklets  $\Upsilon$  from noisy detections; (b) mid-level trajectories  $\Gamma$  obtained via the Hungarian algorithm [9]; (c)  $N$  high-level player trajectories  $\mathcal{T}$  via a cost flow network [27].

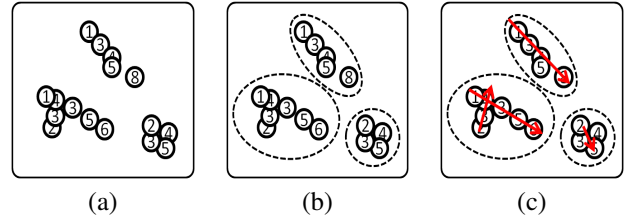


Figure 3. Low-level Tracklets, where each detection is represented as a circle with a frame number. (a) detection responses within a local spatial-temporal volume; (b) identified clusters; (c) RANSAC fitted constant velocity models (red).

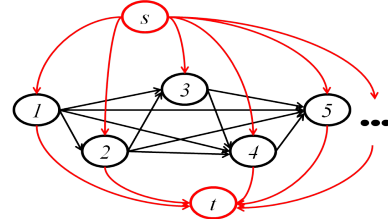


Figure 4. Cost Flow Network. Each vertex  $i$  represents a mid-level trajectory  $\Gamma_i$ . Each directed edge from  $i$  to  $j$  has a cost indicating the negative affinity of associating  $\Gamma_i$  to  $\Gamma_j$ .

the minimum cost path for one unit of flow from  $s$  to  $t$ . The cost  $c_{ij}$  per unit flow from  $i$  to  $j$  indicates the negative affinity, or negative log likelihood that  $\Gamma_j$  is the immediate successor of  $\Gamma_i$ , which we decompose into probabilities in continuity of appearance, time and motion

$$c_{ij} = -\log P(\mathcal{O} | \Gamma_i \rightarrow \Gamma_j) P(\Gamma_i \rightarrow \Gamma_j | \theta) \quad (5)$$

$$= -\log (P_a \cdot P_\tau \cdot P_m). \quad (6)$$

The probability that  $\Gamma_i$  and  $\Gamma_j$  belong to the same team is

$$P_a(\Gamma_i \rightarrow \Gamma_j) = a_i \cdot a_j + (1 - a_i) \cdot (1 - a_j) \quad (7)$$

where  $a_i$  and  $1 - a_i$  are the confidence scores of the mid-level trajectory belonging to team  $A$  and  $B$  respectively.

Let  $t_{i0}$  and  $t_{i1}$  denote the start and end times of  $\Gamma_i$  respectively. If  $\Gamma_j$  is the immediate successor of  $\Gamma_i$ , any non-

zero time gap implies that missed detections must have occurred. Therefore, the probability based on temporal continuity is defined as

$$P_\tau(\Gamma_i \rightarrow \Gamma_j) = \exp(-\lambda(t_{j0} - t_{i1})). \quad (8)$$

Each mid-level trajectory  $\Gamma_i$  has ‘miss-from-the-start’ and ‘miss-until-the-end’ costs on edges  $(s, i)$  and  $(i, t)$  respectively. The weights are computed using (8) for temporal gaps  $(T_0, t_{i0})$  and  $(t_{j1}, T_1)$ , where  $T_0$  and  $T_1$  are the global start and end times of the sequence.

Before describing the form of  $P_m(\Gamma_i \rightarrow \Gamma_j|\theta)$  in more detail, we first discuss how to extract a set of game context features  $\theta$  from noisy detections  $\mathcal{O}$ .

## 4. Game Context Features

In team sports, players assess the current situation and react accordingly. As a result, a significant amount of contextual information is implicitly encoded in player locations. In practice, the set of detected player positions in each frame contains errors, including both missed detections and false detections. We introduce four features (two global and two local) for describing the current game situation with respect to a pair of trajectories that can be extracted from a varying number of noisy detected player locations  $\mathcal{O}$ .

### 4.1. Absolute Occupancy Map

We describe the distribution of players during a time interval using an occupancy map, which is a spatial quantization of the number of detected players, so that we get a description vector of constant length regardless of miss detections and false alarms. We also apply a temporal averaging filter of 1sec on the occupancy map to reduce the noise from detections. The underlying assumption is that players may exhibit different motion patterns under different spatial distributions. For example, a concentrated distribution may indicate a higher likelihood of abrupt motion changes, and smooth motions are more likely to happen during player transitions with a spread-out distribution.

We compute a time-averaged player count for each quantized area. We assume the same distribution could arise regardless of which team is attacking, implying a 180° symmetry in the data. Similarly, we assume a left/right symmetry for each team, resulting in a four-fold compression of the feature space.

Similar to visual words, we use K-means clustering to identify four common distributions (see Fig. 5) roughly characterized as: center concentrated, center diffuse, goal, and corner.

When evaluating the affinity for  $\Gamma_i \rightarrow \Gamma_j$ , we average the occupancy vector over the time window  $(t_{i1}, t_{j0})$  and the nearest cluster ID is taken as the context feature of absolute occupancy  $\theta_{ij}^{(A)} = k \in \{1, \dots, K\}$ .

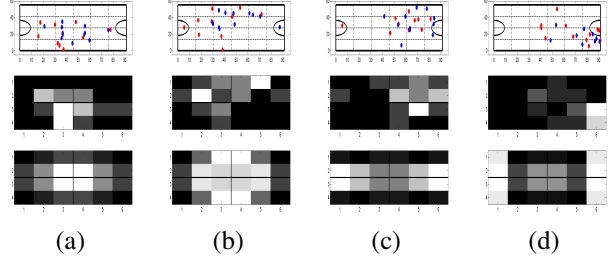


Figure 5. Absolute Occupancy Map. Four clusters are automatically obtained via K-means: (a) center-concentrated, (b) center-diffuse, (c) goal, (d) corner. The rows show: noisy detections (top), estimated occupancy map (middle), and the corresponding cluster center (bottom), which is symmetric horizontally and vertically.

### 4.2. Relative Occupancy Map

The relative distribution of players is often indicative of identity [17]. For example, a forward on the right side typically remains in front and to the right of teammates regardless of whether the team is defending in the back-court or attacking in the front-court. Additionally, the motion of a player is often influenced by nearby players.

Therefore, we define a relative occupancy map specific to each low-level tracklet  $\Upsilon_i$  which quantizes space similarly to the shape context representation: distance is divided into two levels, with a threshold of 4 meters, and direction into four (see Fig. 6). The per-team occupancy count is then normalized to sum to one for both the inner circle and outer ring. Like absolute occupancy maps, we cluster the 16 bin relative occupancy counts (first 8 bins describing same-team distribution, last 8 bins describing opponent distribution) using K-means.

For each pair of  $(\Gamma_i, \Gamma_j)$ , we extract the occupancy vector  $\mathbf{v}_i$  and  $\mathbf{v}_j$ , with cluster ID  $k_i, k_j$ , from the end tracklet of  $\Gamma_i$  and the beginning tracklet of  $\Gamma_j$ . We also compute the Euclidian distance of  $d_{ij} = \|\mathbf{v}_i - \mathbf{v}_j\|_2$ . Intuitively, a smaller  $d_{ij}$  indicates higher likelihood that  $\Gamma_j$  is the continuation of  $\Gamma_i$ . The context feature of relative occupancy is the concatenation of  $\theta_{ij}^{(R)} = (d_{ij}, k_i, k_j)$

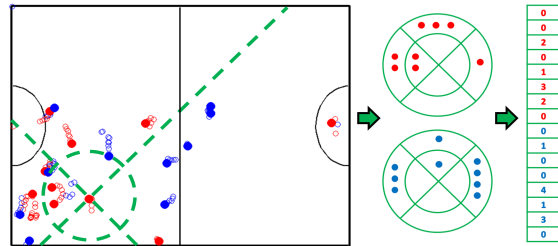


Figure 6. Relative Occupancy Map. The quantization scheme is centered on a particular low-level tracklet  $\Upsilon_i$  at time  $t$ . The same-team distribution and opponent distribution are counted separately.

### 4.3. Focus Area

In team sports such as soccer or basketball, there is often a local region with relatively high player density that moves smoothly in time and may indicate the current or future location of the ball [12,20]. The movement of the focus area in absolute coordinates also strongly correlates to high-level events such as turnovers. We assume the movement of individual players should correlate with the focus area over long time periods, thus this feature is useful for associations  $\Gamma_i \rightarrow \Gamma_j$  with large temporal gaps (when the motion prediction is also less reliable). For example, mid-level trajectory  $\Gamma_i$  in Fig. 7 is more likely to be matched to  $\Gamma_{j1}$  with a constant velocity motion model. However, if the trajectory of the focus area is provided as in Fig. 7, it is reasonable to assume  $\Gamma_i \rightarrow \Gamma_{j2}$  has a higher affinity than  $\Gamma_i \rightarrow \Gamma_{j1}$ .

We estimate the location and movement of the focus area by applying meanshift mode-seeking to track the local center of mass of the noisy player detections. Given a pair of mid-level trajectories ( $\Gamma_i, \Gamma_j$ ), we interpolate the trajectory within the temporal window ( $t_{i1}, t_{j0}$ ) and calculate the variance of its relative distance to the trajectory of the focus area  $\sigma_{ij}$ . We also extract the average speed of the focus area  $v_f$  during the time window, which describes the momentum of the global motion. The focus area context feature is thus set as  $\theta_{ij}^{(F)} = (\sigma_{ij}, v_f)$ .



Figure 7. Focus Area. Kinematic constraints are less reliable across larger time windows. Because player motions are globally correlated, the affinity of two mid-level trajectories over large windows should agree with the overall movement trend of the focus area.

### 4.4. Chasing Detection

Individual players are often instructed to follow or *mark* a particular opposition player. Basketball, for example, commonly uses a one-on-one defense system where a defending player is assigned to follow a corresponding attacking player. We introduce chasing (close-interaction) links to detect when one player is marking another. If trajectories  $\Gamma_i$  and  $\Gamma_j$  both appear to be following a nearby reference trajectory  $\Gamma_k$ , there is a strong possibility that  $\Gamma_j$  is the continuation of  $\Gamma_i$  (assuming the mid-level trajectory of the reference player is continuous during the gap between  $\Gamma_i$  and  $\Gamma_j$ , see Fig. 8).

We identify chasing links by searching for pairs of low-level tracklets ( $\Upsilon_i, \Upsilon_k$ ) that are less than 2 meters apart and moving along similar directions (We use the angular threshold of  $45^\circ$  during the experiment). Let  $\tau_{ij|k}$  be the temporal

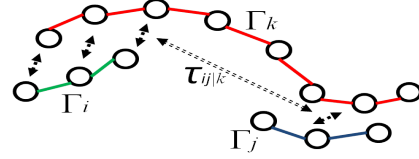


Figure 8. Chasing. If  $\Gamma_i$  and  $\Gamma_j$  both correlate to a nearby trajectory  $\Gamma_k$ , there is a higher likelihood that  $\Gamma_j$  is the continuation of  $\Gamma_i$ .

gap between  $\Gamma_i$ 's last link with  $\Gamma_k$  and  $\Gamma_j$ 's first link with  $\Gamma_k$ , and  $\tau_{ij|k} = \infty$  when there are no links between either  $\Gamma_i$  or  $\Gamma_j$  and  $\Gamma_k$ . The chasing continuity feature  $\theta_{ij}^{(C)}$  that measures whether trajectories  $\Gamma_i$  and  $\Gamma_j$  are marking the same player is given by

$$\theta_{ij}^{(C)} = \min_{k=1, \dots, /i, j} \{\tau_{ij|k}\}. \quad (9)$$

Intuitively, the smaller  $\theta_{ij}$  is, the more likely that  $\Gamma_i, \Gamma_j$  belong to the same player.

## 5. Game Context Conditional Motion Model

Although we have introduced a set of context features  $\theta = \{\theta^{(A)}, \theta^{(R)}, \theta^{(F)}, \theta^{(C)}\}$ , it is nontrivial to design a single fusion method for generating the final motion likelihood score, and features may have varying importance between different sports. For example the chasing-based feature is less important in sports where one-on-one defense is less common. To make our framework general across different sports, we use a pure data-driven approach to learn a motion likelihood based on kinematic (see Tab. 1) and game context features using a Random Decision Forest, which is robust against the overfitting that might occur when using limited training data via bootstrapping, especially when the data is not easily separable due to association ambiguity in the real world. More importantly, a random forest has good local-feature space adaptivity via randomly splitting the feature space at multiple levels of each tree. For example, as confirmed from experiments (Sec.6), the occupancy-feature is more effective at handling short-term association (when feature  $t_g$  is small) and the chasing-feature is more important in connecting trajectories with long temporal gaps ( $t_g$  is big). Random forests are better at automatically capturing such differences compared to other alternatives such as SVM.

symbol	meaning
$t_g$	temporal gap
$e_0$	const-position prediction error
$e_1$	const-velocity prediction error
$e_2$	const-acceleration prediction error
$\Delta \mathbf{v}$	change in velocity

Table 1. Kinematic features

We generate training data by extracting kinematic features  $f_{ij}^{(K)}$  and game context features  $\theta_{ij}$  for all pairs of mid-level trajectories  $(\Gamma_i, \Gamma_j)$ . Using ground truth tracking data, we assign binary labels  $y_{ij} \in \{1, 0\}$  indicating whether the association  $\Gamma_i \rightarrow \Gamma_j$  is correct or not. A random forest containing 500 decision trees is then trained to learn the mapping  $C(f_{ij}^{(k)}, \theta_{ij}) \rightarrow y_{ij}$ . By recursively splitting the data with random subsets of features, our model automatically optimizes local adaptivity, *i.e.*, long gap association and short gap association may be split at different levels and handled with different feature sets.

During the testing stage, the average classification score across all trees provides a continuous affinity score to approximate  $P(\Gamma_i \rightarrow \Gamma_j | \theta) = C(f_{ij}^{(K)}, \theta_{ij})$  in Eqn. 5.

## 6. Experiments

We validate our framework on two sports: field hockey with 20 players and basketball with 10 players. Player detection is transformed from multiple calibrated views using the method in [6] with frame rates of 30 and 25, respectively. We use simple RGB-based color histogram classifiers to estimate the confidence score  $a_i \in [0, 1]$  of tracklet  $i$  belonging to team 0 or 1. We also discard tracklets likely to correspond to the referees and goalies.

### 6.1. Baseline Models and Evaluation metrics

To verify the contribution of the various *GCFs*, we construct 5 models for a quantitative comparison. All models apply hierarchical association and start with the same set of mid-level trajectories  $\Gamma$ . The only difference between the models is the motion affinity used during the final association stage. Model 1 ( $K$ ) only uses kinematic features ( $f^{(K)}$ ) for training, which is equivalent to the combined algorithm of [9, 14, 27]. Model 2-4 use focus area features ( $F$ ), chasing related features ( $C$ ) and occupancy feature ( $A + R$ ), respectively in addition to motion-smoothness features. Model 5 uses all features ( $f^{(K)}, \theta$ ).

We have also examined other features for describing aspects of game context, such as variance of tracklet velocity or team separability. However we found these features to be less effective than the ones described in Sec. 4.

Three errors are commonly evaluated in the multi-target tracking literature: (1) the number of incorrect associations  $N_{err}$ , (2) the number of missed detections  $N_{miss}$ , and (3) the number of false detections  $N_{fa}$ . The Multiple Object Tracking Accuracy measure  $MOTA = 1 - (N_{err} + N_{miss} + N_{fa})/N$  combines all three errors with equal weighting. However the equal weighting de-emphasizes  $N_{err}$  in a hierarchical association framework with a high frame rate. Therefore, we report the individual error sources and normalize for the situation of a known fixed number of objects:  $N_{err}^*$  is an average count of incorrect ID associa-

tions per minute per player;  $P_{miss}$  and  $P_{fa}$  are the proportion of missed and false mid-level trajectory segments of  $\mathcal{T}_n$  as compared to the groundtruth, ranging from 0 to 1.

In addition to overall tracking performance, we also evaluate in isolation the high-level association stage  $\Gamma \rightarrow \mathcal{T}$ , which is the key part of our framework. We report association precision and recall rate, where precision =  $N_{TP}/(N_{TP} + N_{FA})$ , and  $N_{TP}$ ,  $N_{FA}$  are correct/incorrect number of associations of  $\Gamma_i \rightarrow \Gamma_j$ . We define recall =  $1 - T_{miss}/T_{gap}$ , where  $T_{gap}$  is the accumulation of temporal gaps  $t_{gap}$  between high-level associations, and  $T_{miss}$  is the total length of mid-level trajectories  $\Gamma_i$  being missed. The motivation is to exclude miss-associations in previous stages. An illustration of these metrics is given in Fig. 9. Finally, we also report the statistics of average length tem-

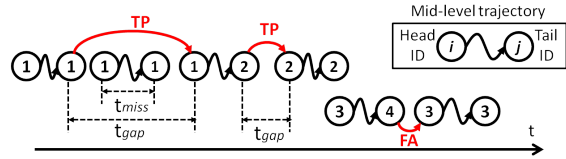


Figure 9. Demonstration of evaluation metrics for high-level association (red).

poral gap  $\bar{t}_{gap}$  being correctly associated during the high-level association, which reflects the algorithm’s ability to associate trajectories with long-term misses.

### 6.2. Field Hockey Dataset

We generated and labeled 6 field hockey sequences for a total length of 29 minutes, from 3 games played by different teams. The average player detection miss and false-alarm rates are 14.0% and 10.3%, respectively, or the multi-target detection accuracy  $MODA = 1 - (N_{miss} + N_{fa})/N = 0.75$ . Our first experiment uses as much training data as possible: testing one sequence and using the remaining five for training.

The introduction of each individual *GCF* achieves better performance, and using all *GCFs* generally produces the best performance (see Tab. 2).

The  $\bar{t}_{gap}$  column of the hockey sequences in Tab. 2 shows how the focus area feature achieves the maximum average-temporal-gap between correct associations indicating its advantage in dealing with long-term misses. On the other hand, the absolute and relative player distributions feature has the smallest temporal gap, indicating it is more useful for short-term misses.

Furthermore, as can be seen from Tab. 2, all methods are good in terms of low false-alarm rate. Thus the major difference in their performances is reflected in the terms for incorrect association  $N_{err}^*$  and miss association  $P_{err}$ .

We can also introduce a weighting  $w_m$  on motion likelihood relative to the appearance likelihood into the objective

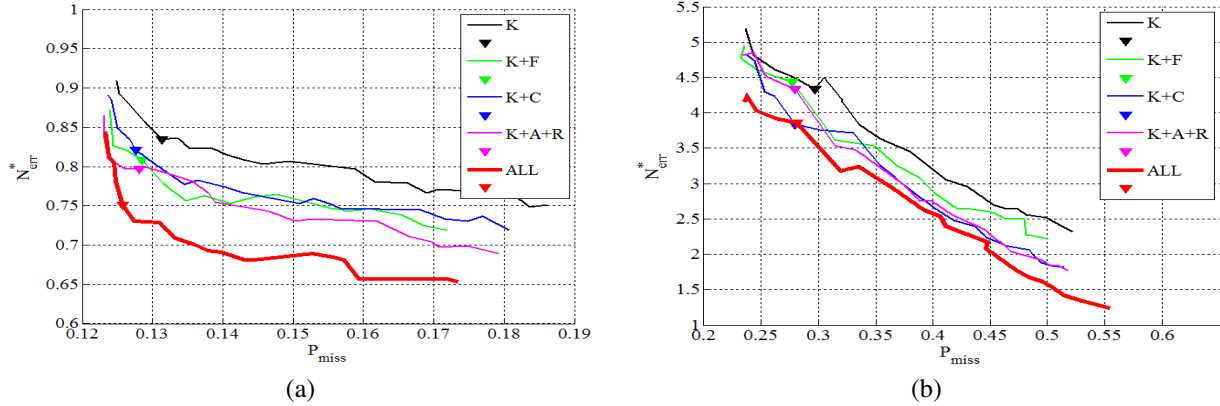


Figure 10. Trade-off curve between  $P_{miss}$  and  $N_{err}^*$  for (a) field hockey sequences and (b) basketball sequences.  $N_{err}^*$  is averaged association error per minute per person. The triangle marks indicate the default operating point ( $w_m = 1$  in Eqn.10). Our proposed method using all *GCFs* achieves more than 10% of improvements on both cases.

function of Eqn. 1, where  $w_m$  plays an essential role in the trade-off between miss-associations and false associations:

$$\log P(\mathcal{T}|\mathcal{O}, \theta) = \log P(\mathcal{O}|\mathcal{T}) + w_m \cdot \log P(\mathcal{T}|\theta) + c. \quad (10)$$

Instead of the default setting of  $w_m = 1$ , a lower weight for the motion likelihood ( $w_m < 1$ ) gives higher priority to optimizing the observation likelihood  $P(\mathcal{O}|\Gamma)$ , e.g., less players missing. On the other hand, a higher weighting with  $w_m > 1$  encourages smoother motions to be associated and results in fewer false alarms but also fewer true positives. As we vary  $w_m$  from 0.2 to 3, the trade-off curves are plotted in Fig. 10(a).

We also conduct an experiment studying the cross-game-generalization of the *GCFs*. Instead of testing 1 sequence trained on the other 5, we perform all pairwise combinations (30 in total) of 1 sequence training with 1 other sequence testing. We then evaluate the resulting statistics for same-game learning and different-game learning respectively, as summarized in Tab. 3.

It can be seen that the introduction of *GCFs* again improves the result both in the case of same-game and cross-game learning, yet this time the amount of training data used is much smaller (4 minutes on average). On the other hand, same-game learning outperforms cross-game learning in terms of generalization, which matches our intuition that the game context features are more similar within the same game with the same players, e.g., the team distribution/tactics and the velocity/acceleration of players are more consistent.

### 6.3. Basketball Dataset

We also conduct the same evaluation on a basketball dataset of 4 sequences for a total length of more than 5 minutes. The dataset is more challenging due to a higher player density and less training data. Each sequence is tested while

using the other 3 sequences for training. The average testing performance is reported in the trade-off curve of Fig. 10(b) and Tab. 2. As can be seen, the chasing feature is much

Field Hockey					
	<i>K</i>	<i>K, F</i>	<i>K, C</i>	<i>K, A, R</i>	<i>ALL</i>
$N_{err}^*$	.84	.81	.82	.80	<b>.75</b>
$P_{miss}$	.131	.129	.128	.128	<b>.126</b>
$P_{fa}$	.032	.032	.032	.033	<b>.031</b>
precision	.69	.71	.70	.71	<b>.75</b>
recall	.97	.97	.97	<b>.98</b>	.97
$\bar{t}_{gap}$ (sec)	3.68	3.97	3.56	3.62	3.95
Basketball					
	<i>K</i>	<i>K, F</i>	<i>K, C</i>	<i>K, A, R</i>	<i>ALL</i>
$N_{err}^*$	4.33	4.43	<b>.380</b>	4.32	3.81
$P_{miss}$	.30	.280	<b>.280</b>	.280	.281
$P_{fa}$	.027	.031	.024	.025	<b>.018</b>
precision	.65	.67	.71	.68	<b>.71</b>
recall	.99	.99	.99	.99	<b>.99</b>
$\bar{t}_{gap}$ (sec)	3.26	3.99	5.09	3.60	3.81

Table 2. Quantitative evaluations

same game	<i>K</i>	<i>K, F</i>	<i>K, C</i>	<i>K, A, R</i>	<i>ALL</i>
$N_{err}^*$	.81	.84	.78	.78	<b>.77</b>
$P_{miss}$	.141	<b>.133</b>	.134	.136	.134
$P_{fa}$	.034	.034	.033	.034	<b>.033</b>
cross game	<i>M</i>	<i>K, F</i>	<i>K, C</i>	<i>K, A, R</i>	<i>ALL</i>
$N_{err}^*$	1.24	1.23	1.19	1.17	<b>1.14</b>
$P_{miss}$	.130	.125	.127	.126	<b>.124</b>
$P_{fa}$	.036	.034	.035	.034	<b>.034</b>

Table 3. Comparison of same/cross game learning (Hockey)

more important for basketball sequences, indicating that one-on-one defensive situations occur more frequently in basketball than field hockey.

## 7. Summary

In this work, we use hierarchical association to track multiple players in team sports over long periods of time. Although the motions of players are complex and highly correlated with teammates and opponents, the short-term movement of each player is often reactive to the current situation. Using this insight, we define a set of game context features and decompose the motion likelihood of all players into independent per-player models contingent on game state. Higher-order inter-player dependencies are implicitly encoded into a random decision forest based on track and game context features. Because the conditioned model decomposes into pairwise terms, our formulation remains efficiently solvable using cost flow networks. We validate our approach on 30 minutes of international field hockey and 10 minutes of college basketball. In both sports, motion models conditioned on game context features consistently improve tracking results by more than 10%.

**Acknowledgment** This work is funded partially under NSF grants IIS-1248076 and IIS-1144938.

## References

- [1] S. Ali and M. Shah. Floor fields for tracking in high density crowd scenes. In *ECCV*, 2008. 1, 2
- [2] A. Andriyenko and K. Schindler. Multi-target tracking by continuous energy minimization. In *CVPR*, 2011. 2
- [3] A. Andriyenko, K. Schindler, and S. Roth. Discrete-continuous optimization for multi-target tracking. In *CVPR*, 2012. 2
- [4] W. Brendel, M. Amer, and S. Todorovic. Multiobject tracking as maximum weight independent set. In *CVPR*, 2011. 1, 2
- [5] Y. Cai, N. de Freitas, and J. Little. Robust visual tracking for multiple targets. In *ECCV*, 2006. 2
- [6] P. Carr, Y. Sheikh, and I. Matthews. Monocular object detection using 3d geometric primitives. In *ECCV*, 2012. 6
- [7] R. Collins. Multi-target data association with higher-order motion models. In *CVPR*, 2012. 1, 2
- [8] W. Du, J. Hayet, J. Piater, and J. Verly. Collaborative multi-camera tracking of athletes in team sports. In *Workshop on Computer Vision Based Analysis in Sport Environments*, 2006. 2
- [9] C. Huang, B. Wu, and R. Nevatia. Robust object tracking by hierarchical association of detection responses. In *ECCV*, 2008. 2, 3, 6
- [10] H. Jiang, S. Fels, and J. Little. A linear programming approach for multiple object tracking. In *CVPR*, 2007. 2
- [11] Z. Khan, T. R. Balch, and F. Dellaert. An mcmc-based particle filter for tracking multiple interacting targets. In *ECCV*, 2004. 2
- [12] K. Kim, M. Grundmann, A. Shamir, I. Matthews, J. Hodgins, and I. Essa. Motion fields to predict play evolution in dynamic sport scenes. In *CVPR*, 2010. 2, 5
- [13] M. Kristan, J. Pers, M. Perse, and S. Kovacic. Closed-world tracking of multiple interacting targets for indoor-sports applications. *CVIU*, 113(5):598–611, 2009. 2
- [14] Y. Li, C. Huang, and R. Nevatia. Learning to associate: Hybrid-boosted multi-target tracker for crowded scene. In *CVPR*, 2009. 6
- [15] W.-L. Lu, J.-A. Ting, K. Murphy, and J. Little. Identifying players in broadcast sports videos using conditional random fields. In *CVPR*, 2011. 2
- [16] C. J. Needham and R. D. Boyle. Tracking multiple sports players through occlusion, congestion and scale. In *BMVC*, 2001. 2
- [17] P. Nillius, J. Sullivan, and S. Carlsson. Multi-target tracking - linking identities using bayesian network inference. In *CVPR*, 2006. 2, 4
- [18] S. Pellegrini, A. Ess, K. Schindler, and L. van Gool. You'll never walk alone: Modeling social behavior for multi-target tracking. In *ICCV*, 2009. 1, 2
- [19] A. Perera, C. Srinivas, A. Hoogs, G. Brooksby, and W. Hu. Multi-object tracking through simultaneous long occlusions and split-merge conditions. In *CVPR*, 2006. 2
- [20] F. Poiesi, F. Daniyal, and A. Cavallaro. Detector-less ball localization using context and motion flow analysis. In *ICIP*, 2010. 5
- [21] M. Rodriguez, S. Ali, and T. Kanade. Tracking in unstructured crowded scenes. In *ICCV*, 2009. 2
- [22] C. Santiago, A. Sousa, M. Estriga, L. Reis, and M. Lames. Survey on team tracking techniques applied to sports. In *AIS*, pages 1–6, 2010. 2
- [23] H. Shitrit, J. Berclaz, F. Fleuret, and P. Fua. Tracking multiple people under global appearance constraints. In *ICCV*, 2011. 1
- [24] J. Xing, H. Ai, L. Liu, and S. Lao. Multiple player tracking in sports video: A dual-mode two-way bayesian inference approach with progressive observation modeling. *Trans. Img. Proc.*, 20(6):1652–1667, 2011. 2
- [25] B. Yang and R. Nevatia. Multi-target tracking by online learning of non-linear motion patterns and robust appearance models. In *CVPR*, 2012. 1
- [26] T. Yu and Y. Wu. Collaborative tracking of multiple targets. In *CVPR*, 2004. 2
- [27] L. Zhang, Y. Li, and R. Nevatia. Global data association for multi-object tracking using network flows. In *CVPR*, 2008. 1, 2, 3, 6
- [28] T. Zhang, B. Ghanem, and N. Ahuja. Robust multi-object tracking via cross-domain contextual information for sports video analysis. In *ICASSP*, 2012. 2
- [29] X. Zhao, D. Gong, and G. Medioni. Tracking using motion patterns for very crowded scenes. In *ECCV*, 12. 1, 2